HHS Public Access

Author manuscript

Dev Biol. Author manuscript; available in PMC 2024 March 01.

Published in final edited form as:

Dev Biol. 2023 March ; 495: 92–103. doi:10.1016/j.ydbio.2023.01.006.

Drosophila transmembrane protein 214 (dTMEM214) regulates midgut glucose uptake and systemic glucose homeostasis

Yue Li[1,€], **Weidong Wang**[2], **Hui-Ying Lim**[1,*]

[1]Department of Physiology, University of Oklahoma Health Science Center, Oklahoma City, Oklahoma, USA

[2]Department of Medicine, Section of Endocrinology, University of Oklahoma Health Sciences Center, Oklahoma City, Oklahoma, USA

Abstract

The availability of glucose transporter in the small intestine critically determines the capacity for glucose uptake and consequently systemic glucose homeostasis. Hence a better understanding of the physiological regulation of intestinal glucose transporter is pertinent. However, the molecular mechanisms that regulate sodium-glucose linked transporter 1 (SGLT1), the primary glucose transporter in the small intestine, remain incompletely understood. Recently, the *Drosophila* SLC5A5 (dSLC5A5) has been found to exhibit properties consistent with a dietary glucose transporter in the *Drosophila* midgut, the equivalence of the mammalian small intestine. Hence, the fly midgut could serve as a suitable model system for the study of the in vivo molecular underpinnings of SGLT1 function. Here, we report the identification, through a genetic screen, of *Drosophila* transmembrane protein 214 (dTMEM214) that acts in the midgut enterocytes to regulate systemic glucose homeostasis and glucose uptake. We show that dTMEM214 resides in the apical membrane and cytoplasm of the midgut enterocytes, and that the proper subcellular distribution of dTMEM214 in the enterocytes is regulated by the Rab4 GTPase. As a corollary, *Rab4* loss-of-function phenocopies *dTMEM214* loss-of-function in the midgut as shown by a decrease in enterocyte glucose uptake and an alteration in systemic glucose homeostasis. We further show that dTMEM214 regulates the apical membrane localization of dSLC5A5 in the enterocytes, thereby revealing dTMEM214 as a molecular regulator of glucose transporter in the midgut.

Graphical Abstract

[*]To whom correspondence should be addressed. huiying-lim@ouhsc.edu.
[€]Current address: Zhejiang University, Hangzhou, China

Declarations of interest

None

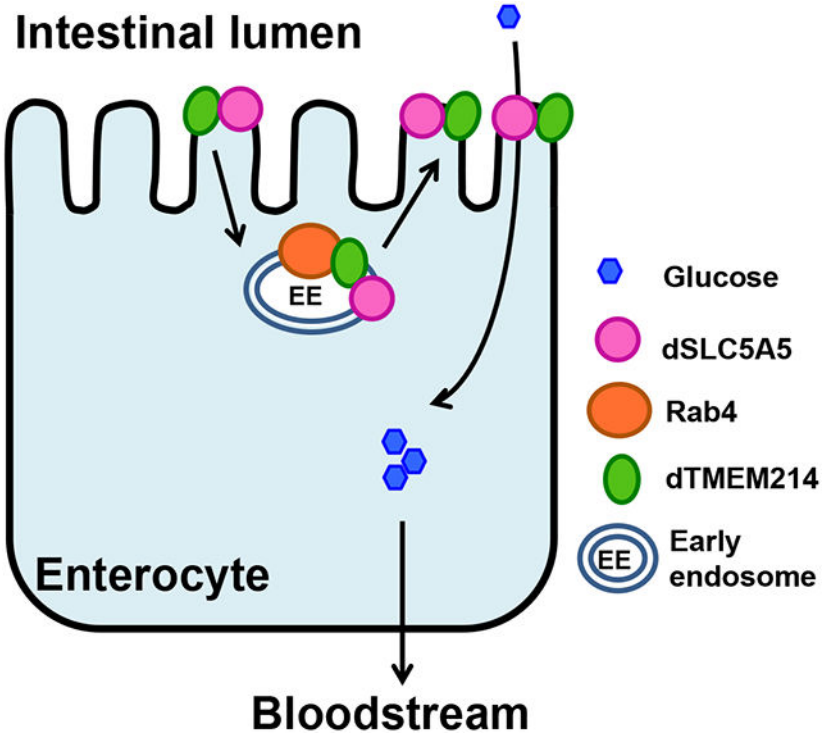

Keywords

Transmembrane protein; Rab4; Solute carrier 5A; glucose transporter; glucose absorption; intestinal enterocytes

Introduction

Excessive sugar intake induces glucose intolerance and insulin resistance, conditions that give rise to metabolic disorders such as Type 2 diabetes. A better understanding of the molecular mechanisms that control glucose uptake and metabolism could provide new therapeutic strategies to alleviate diabetes and other metabolic syndromes. Glucose transport is mediated by both sodium dependent and facilitated transport. The sodium-dependent glucose cotransporters form a family of proteins named SGLT which are encoded by the *SLC5A* genes, while the sodium-independent glucose transporters form the GLUT family of proteins encoded by the *SLC2A* genes (Sedzikowska and Szablewski, 2021). Absorption of dietary glucose in the intestinal cell is mediated by SGLT1, which is enriched in the apical or brush border membrane of the mature enterocytes (Roder et al., 2014). More recently, *Drosophila SLC5A5 (dSLC5A5)*, which is homologous to the human *SLC5A* family, has been shown to mediate glucose uptake in the enterocytes of the fly midgut (Li et al., 2021), a tissue that is functionally analogous to the human small intestine. The identification of such a previously-unrecognized function of dSLC5A5 suggests that the fly midgut could serve as a relevant model system to identify important players that direct glucose uptake in the enterocytes. Because of conservation of genes between *Drosophila* and mammals (Reiter et al., 2001), it is likely that the proteins that regulate midgut glucose uptake may

also serve similar functions in the small intestine, which would contribute towards a better understanding of the molecular basis of glucose absorption in physiological or pathological conditions in mammals.

In order to exert their proper function, glucose transporters need to be properly transported to the plasma membrane in the intestine. A number of proteins are known to be involved in the apical/basolateral trafficking of proteins in polarized epithelial cells. Rab proteins are members of the Rab GTPase family with 66 and 26 members in humans and *Drosophila*, respectively (Chan et al., 2011; Dunst et al., 2015; Gillingham et al., 2014; Jin et al., 2012). Among the 26 *Drosophila* genes, 23 have direct orthologs in humans that are at least 50% identical at the protein level, indicating high evolutionary conservation (Chan et al., 2011; Kohrs et al., 2021). Many Rab proteins are localized in the cytosolic side of plasma membrane and function to regulate different steps of intracellular membrane trafficking - vesicle budding, transport, uncoating, tethering, docking, and fusion – in all cell types (Barbero et al., 2002; Carroll et al., 2001; Grigoriev et al., 2007; Grosshans et al., 2006; Hutagalung and Novick, 2011; Jordens et al., 2001; Lee et al., 2011; Nielsen et al., 2000; Rojas et al., 2008; Strom et al., 2002). In agreement with their roles in regulating intracellular vesicular transport system, alterations in the levels of the Rab GTPases have been associated with various human diseases ranging from cancer to infectious diseases. Localized in the early sorting and recycling endosomes, Rab4 regulates early endosomal traffic such as membrane recycling (Cormont et al., 2001; Fouraux et al., 2004; van der Sluijs et al., 1992b). Rab5 and Rab7 are involved in cargo selection through recruitment of a retromer complex of nexin dimer and Vps26/29/35 trimer to the endosomes (Rojas et al., 2008). Other Rabs such as Rab 11 and Rab27a function to recruit effectors that facilitate vesicle movement along the cytoskeletal elements (Casavola et al., 2008; Grigoriev et al., 2007; Jordens et al., 2001; Strom et al., 2002). Interestingly, several Rab GTPases have been implicated in governing the subcellular distribution of glucose transporters. For instance, Rab8 is required for the proper localization of SGLT1 in the apical membrane of small intestinal epithelial cells (Sato et al., 2007) whereas Rab4 is involved in the translocation of GLUT4 to the plasma membrane under conditions of insulin stimulation in mammalian adipocytes and skeletal muscle cells (Aledo et al., 1995; Cormont et al., 1996; Mari et al., 2006; Ricort et al., 1994; Shibata et al., 1997). Rab4 has been proposed to act with other proteins in regulating glucose transporter subcellular trafficking in the adipocytes. For instance, overexpression of Rabip4, a Rab4 effector (Cormont et al., 2001), increases glucose transport induced by insulin in the 3T3-L1 adipocytes (Cormont et al., 2001), suggesting that Rab4 and Rabip4 cooperate in insulin-induced Glut4 translocation. Furthermore, Rab4 directly interacts with Syntaxin 4 and both are implicated in insulin-induced GLUT4 translocation in the adipocytes (Li et al., 2001). One can envision that Rab4 might also act with other partners to direct the subcellular trafficking of glucose transporters in tissues beyond the adipose tissue, such as in the small intestine. However, it is by far unknown whether and how Rab4 could play a role in regulating the subcellular distribution of glucose transporter in the small intestine.

The transmembrane protein (TMEM) family comprises proteins that bear a conserved 450-amino acid domain and are typically anchored to lipid bilayers, including the plasma membrane and those of membrane-bound organelles [mitochondria, golgi

apparatus, endoplasmic reticulum (ER), and peroxisome]. The TMEMs are implicated in multiple cellular processes including cell proliferation, migration, and survival and their dysregulations are associated with human diseases including cancer (Cobbold et al., 2003; Schmit and Michiels, 2018). A member of the TMEM family, Transmembrane protein 214 (TMEM214), was reported to mediate ER-induced apoptosis in a cultured cell study (Li et al., 2013). TMEM214 has also been implicated in cellular mRNA degradation (Lehner and Sanderson, 2004). In addition, the *Drosophila* orthologue of human TMEM214, dTMEM214, was found to be involved in hyperoxia-induced oxidative stress regulation (Zhao et al., 2010). In this study, we further identify a previously-unrecognized role of dTMEM214 in regulating systemic glucose homeostasis. We show that dTMEM214 resides in the midgut enterocytes, and that the subcellular distribution of TMEM214 in the enterocytes is regulated by Rab4. Notably, depletion of dTMEM214 or Rab4 in the enterocytes inhibits glucose uptake and perturbs systemic glucose homeostasis. We further provide evidence supporting that dTMEM214 regulates the subcellular distribution of the glucose transporter dSLC5A5 in the enterocytes, which sheds light into the mechanistic action of dTMEM214 in maintaining normal systemic glucose metabolism.

Materials and Methods

Fly Stocks and transgenic lines

All fly stocks were maintained at 25°C on standard medium unless otherwise stated. The following strains were used in this study: w^{1118} (BDSC BL6326), *Actin-Gal4* (BDSC BL3954), *Hsp70-Gal4* (BDSC BL2077), *Caudal (Cad)-Gal4* (BDSC BL3042), *UAS-dTMEM214*^{RNAi} (BDSC BL33751), *UAS-dSLC5A1*^{RNAi} (BDSC BL37273), *UAS-Rab4*^{RNAi} (BL33757), *UAS-Rab4-mRFP* (BL8505), *UAS-Rab5*^{RNAi} (BL34832), *UAS-Rab7*^{RNAi} (BL27051), *UAS-Rab11*^{RNAi} (BL27730), *abo[1]* (BL2525), *aub[HN2]* (BL8517), *UAS-GFP*^{nuclear} (gift from Wan-Hee Yoon, OMRF). The deficiency lines include the Bloomington deficiency kit for chromosome 2L (DK2L) and include the *Df(2L)BSC145* deficiency (BL9505). DK2L contains 102 stocks with molecularly defined genomic deletions generated primarily by two groups, Exelixis and DrosDel (Cook RK Genome Biol 2012). Among the deficiency lines tested, we have identified at least 8 deficiency lines that exhibited increases in systemic glucose levels compared to w^{1118} on either or both ND and HSD (*Df(2L)ED441, Df(2L)ED8142, Df(2L)Exel6009, Df(2L)BSC692, Df(2L)Exel6012, Df(2L)ED385, Df(2L)BSC159, Df(2L)BSC892)* and at least 10 deficiency lines (other than the *Df(2L)BSC145* deficiency) that exhibited decreases in systemic glucose levels compared to w^{1118} on either or both ND and HSD (*Df(2L)BSC147, Df(2L)BSC188, Df(2L)Exel7011, Df(2L)ED690, Df(2L)BSC169, Df(2L)BSC204, Df(2L)ED7853, Df(2L)Exel8038, Df(2L)BSC214, Df(2L)BSC227*). The *dTMEM214* mutant lines (*d11065, f00442, f05566, f07745, f07748*) were obtained from Exelixis at Harvard Medical School. The *dTMEM214-Gal4* strain was obtained from the Kyoto Drosophila Stock Center (104232; DGRC). The *UAS-dSLC5A5-FLAG* line was described in (Li et al., 2021). The *Myo1A-Gal4* fly line was a gift from Dr. Bruce Edgar (University of Utah, Salt Lake City). The full length MGC *dTMEM214* cDNA (clone ID: 4814193, DGRC) was cloned into the *pUAST* vector and the construct was microinjected into germline for the generation of the *UAS-dTMEM214* transgenic flies (Bestgene, CA).

Feeding regimen

Parental flies (female n=15-20, male n=5-10) were removed from normal diet (ND) after laying eggs for ~2 days. The progenies were reared on ND till newly eclosed adult stages before being transferred to new vials with fresh ND or high sugar diet (HSD). Progenies were collected for different analyses at 1-week post-eclosion.

Glucose assay

Whole flies (4 males and 4 females per genotype) or midguts dissected from 12 female flies of each genotype were homogenized in 100 μl PBS + 0.05% Triton X-100. After 10 minutes of centrifugation (15,600×*g*, 4°C), 2 μl supernatant was used to detect protein concentration (μg/μl) (Bradford assay). The rest of the supernatant was heated for 10 minutes at 70°C, followed by 3-minute centrifugation (15,600×*g*, 4°C). The second time supernatant (20 μl) was diluted in 80 μl distilled water and incubated with 900 μl Glucose Reagent (Thermo Scientific, #TR15421) for 3 minutes at 37°C. The absorbance at 340 nm was measured and the glucose content (μg/μl) was calculated using a glucose standard curve. The final glucose level in ug/ug protein was calculated from the sample protein concentration.

Hemolymph trehalose assay

One-week old female flies (n=30-40) were starved for 6 hours (only supplied with distilled water) before hemolymph collection. Flies with holes punched in the thorax by needles (27G ½") were transferred to a 0.5 ml microfuge tube that has a small hole at the bottom and filled with a layer of glass wool. The tube was then placed in a 1.5 ml microfuge tube to be centrifuged for 5 minutes (9,000×*g*, 4°C). The hemolymph (1 μl) was carefully removed from the collection tube, diluted in 99 μl trehalase buffer (TB) (5 mM Tris, pH 6.6,137 mM NaCl, 2.7 mM KCl) and immediately heated at 70°C for 10 minutes to inactivate the endogenous trehalase. After heating, 40 μl diluted hemolymph was mixed with 60 μl TB while another 40 μl was added into 60 μl TB with trehalase (TS) [15 μl trehalase (Sigma; T8778-1UN) in 1 ml TB] to convert trehalose to glucose. After 24 hours incubation at 37°C, glucose contents (μg/μl) in TB and TS samples were detected with Glucose Reagent. The additional amount of glucose in the TS sample compared to the TB sample was considered to be digested from trehalose.

Glycogen assay

The fat body of 1-week old female flies (n=12 per genotype) were dissected, homogenized in 10μl PBS, and centrifuged at 15,600×*g* for 10 minutes at 4°C. 3μl of supernatant was then used to detect protein concentration and the rest was heated for 10 min at 70°C. After 3 minutes centrifuge (15,600×*g*, 4°C) the heat-treated supernatant was transferred in to a new microfuge tube. 30 μl of each supernatant was mixed with 70 μl PBS while another 30 μl was added into 70 μl PBS with amyloglucosidase [4 μl amyloglucosidase (Sigma A1602; 25mg) in 1 ml PBS] in order to break down glycogen into glucose. Samples were incubated at 37°C for overnight before glucose measurement by Glucose Reagent. Glycogen content (μg/μl) of each sample was determined by subtracting glucose content in PBS-treated sample from glucose content in amyloglucosidase-treated sample.

Immunostaining

Midguts were dissected in PBS and fixed with 10% formaldehyde for 10 mins at room temperature. The fixed tissues were then subjected to three rounds of 15 minute-each wash with 0.1% PBST (0.1% Triton X-100 in PBS) and blocked with 5% donkey serum (Jackson ImmunoResearch Laboratories, 107-000-121) for 1 hour at room temperature followed by incubation with primary antibodies in 5% donkey serum at 4°C. The tissues were then washed three times, 10 mins each time in 0.1% PBST, followed by 2 hours incubation with alexa-fluor-conjugated secondary antibodies (Jackson Immunoresearch) in 0.1% PBST at room temperature. After washing as before, tissues were mounted in Vectashield media (Vector Laboratories, Inc.) and viewed under a laser scanning confocal microscope (Olympus FV1000). The primary antibodies used for immunostaining are mouse anti-FLAG [(1:500, Sigma (F1804)], guinea pig anti-Myo7a (1:1000, gift from Dr. Dorothea Godt, University of Toronto, Canada), Alexa Fluor 488 phalloidin [Invitrogen (A12379) 10μM] and anti-dTMEM214 (1:50). The dTMEM214 antibody was raised as a polyclonal antibody in rabbits against the N-terminal amino acid sequence KQKNLDKKVSAHNEC. The secondary antibodies are donkey anti-mouse Cy3 (1:150, Jackson Immunoresearch) and donkey anti-rat Cy3 (10μM, Jackson Immunoresearch).

Western blotting

Ten flies were homogenized in 100 μl PBST (0.1% Triton X-100) with protease inhibitors and centrifuged at 15,600×*g* for 15 minutes at 4°C and the supernatant collected for western blot. 40 μg protein of each sample was loaded into Novex NuPAGE 10% Bis-Tris Gels (Invitrogen, NP0301BOX) and then transferred to nitrocellulose membranes (Invitrogen, LC2001). Membranes were incubated with primary antibodies: rabbit anti-dTMEM214 (1:500) and anti-β-actin (Rabbit polyclonal 1:3000, GeneTex) overnight at 4°C after 1-hour blocking in PBST with 5% non-fat milk at room temperature. Membranes were then washed with PBST and incubated with horseradish peroxidase-conjugated secondary antibodies (anti-mouse and anti-rabbit, Perkin Elmer) for one hour at room temperature. ECLTM Western Blotting Detection Reagents (GE Healthcare, RPN2209) was utilized to visualized protein bands.

Ex vivo glucose uptake assay

Following 6-hour starvation with deionized water only, midguts were dissected in ice-cold PBS from 1-week old female flies. A horizontal incision was made to the posterior midgut with the tip of needles (27G ½”) to expose the enterocytes. Samples were incubated with 300 μM 2-NBDG (2-(N-(7-Nitrobenz-2-oxa-1,3-diazol-4-yl)Amino)-2-Deoxyglucose for 45 mins at room temperature. After three brief washes with PBS, tissues were fixed in 3.7% formaldehyde for 15 minutes, followed by three 5-min washes with PBS. Midguts were mounted in Vectashield media.

In vivo glucose uptake assay

Following 6-hour starvation with deionized water only, 1-week old female flies were fed with 2-NBDG (750 μM in PBS) for 45 minutes at room temperature. Midguts were then

dissected in ice-old PBS, fixed in 3.7% formaldehyde for 15 mins, washed in PBS for 3 times (5 minutes per time), and mounted in Vectashield media.

Real-time quantitative PCR (qRT-PCR)

Total RNA was extracted from tissues in adult flies (n=15 per genotype) using Trizol Reagent (Ambion). cDNA using oligo(dT) were synthesized from total RNA (500ng to 1 μg each) with Superscript III reverse transcriptase (Invitrogen). qPCR amplification reactions were performed in triplicates, by mixing 1 μl of RT product with 10 μl of SYBR qPCR Mastermix (Qiagen) containing the appropriate primers (345 nM of forward primer and 345 nM of reverse primer). Thermal cycling and fluorescence monitoring were performed in a CFX96 (Bio-rad) using the following cycling conditions: 95°C for 10 minutes and (95°C for 15 seconds, 60°C for 1 minute) x 40. Values were normalized with *Rpl14*. Primers used are as follows:

Actin-5C F: 5'- GGCGTAATGGTAGGAATGGGACAAA −3'

R: 5'- GTGCTTTCTCTCTACGCCTCCGG −3'

dTMEM214 F: 5'- AAAAAGAAATGCGGATGCTG −3'

R: 5'- AAAGCTTCGATTTTGCCAGA −3'

Food intake measurement

Food intake for adult flies was measured using the capillary feeder (CAFE) assay as described previously (Liu et al., 2019). Briefly, 1-week old adult female flies (N = 10) were weighed and then starved for 16 hours before being transferred to the CAFE chambers comprising an empty food vial with wet cotton at the bottom to maintain humidity. One 100 μL (1 μL/mm) capillary tube with liquid food (400 mM sucrose solution + blue dye) was inserted into each chamber through a cotton plug. Flies were fed at room temperature for 6 hours, after which total liquid food consumption was calculated as the length of colored food at 0 hour minus the length of colored food at 6 hours within the capillary tube (μL). A control liquid food chamber without flies was used for the correction of liquid food evaporation (μL'). Total food consumption (ΔL-ΔL') in μl was normalized to weight (g). Food consumption per fly was calculated by further dividing the normalized total food consumption by 10.

Sequence analyses

Multiple sequence alignment analysis was performed by UniProt (Pundir et al., 2017) with protein sequences in FASTA format extracted from the National Center for Biotechnology Information (NCBI).

Statistical Analysis

All data were presented as the mean ± SEM of the indicated number of replicates. Pairwise comparison *p*-values involving only 2 groups (control and experimental groups) were analyzed using unpaired, two-tailed, Student's *t*-test. Statistical analysis was performed using Microsoft Excel (2016). $p < 0.05$ was considered statistically significant.

Results

Genetic screening identifies dTMEM214 as a regulator of glucose homeostasis under normal and high sugar diets

To identify novel components involved in the regulation of glucose metabolism, we performed a haplo-insufficiency screen for genes that could alter high sugar diet (HSD)-mediated glucose dysregulation in *Drosophila*. For that, we developed a feeding regimen that significantly increased systemic and circulating sugar levels in the wild-type (w^{1118}) flies reared on HSD compared to their normal diet (ND)-reared counterparts (Li et al., 2021). The HSD-fed flies also developed insulin resistance as well as obesity (Li et al., 2021), which altogether provide evidence that our HSD feeding regimen generates a *Drosophila* model of diet-induced dysregulation of glucose metabolism. Using the same feeding regimen to screen a collection of deficiency lines (see Materials and Methods), we identified a chromosomal 2L deficiency line, *Df(2L)BSC145* line, that displayed significant decreases in systemic glucose levels compared to w^{1118} flies on both ND and HSD (Figures 1A and 1B). We determined that food intake was comparable between the *Df(2L)BSC145* line and w^{1118} flies on both ND and HSD (Figure 1C), suggesting that food consumption does not contribute to the decreased systemic sugar levels in the *Df(2L)BSC145* line. According to the Flybase database, the *Df(2L)BSC145* deficiency uncovers ten genes including *CG33129*, which encodes *dTMEM214* (Figure 1A). To determine if any of the ten genes in the *Df(2L)BSC145* line regulates systemic glucose levels, we utilized a candidate-based approach whereby we genetically interfered with the function of several of those genes followed by the assessment of systemic glucose level decrease. Among the three genes uncovered within *Df(2L)BSC145* (CG33129/dTMEM214, *abo[1], aub[HN2]*; Figure S1A), we detected no significant difference in systemic glucose levels between the w^{1118} flies and *abo[1]* flies or between the w^{1118} flies and *aub[HN2]* flies on ND (Figure S1B). On the other hand, we found that several homozygous mutants of *dTMEM214* exhibited significantly decreased whole-body glucose content compared to the w^{1118} flies on ND (Figure 1D). dTmem214 is a transmembrane protein that shares between 25 to 31 percent identity to orthologs in human, dog, rabbit, mouse, chicken, frog, and zebrafish (Figure S2). As the *dTMEM214* mutants phenocopy the *Df(2L)BSC145* line (see Figures 1B and 1D), we further examined the role of DTMEM214 on systemic glucose homeostasis. We next performed RNA interference (RNAi)-mediated whole-body knockdown of *dTMEM214*.using the ubiquitous *Actin-Gal4* driver (*Act-Gal4>dTMEM214*^{RNAi}; Figure S3A) and observed significantly lowered systemic glucose levels relative to the control flies (*UAS-dTMEM214*^{RNAi}) under both ND and HSD (Figure S3B). The decrease in systemic glucose levels associated with dTMEM214 inhibition was not due to changes in feeding behavior, as the *Act-Gal4>dTMEM214*^{RNAi} flies displayed similar food consumption as the control flies on ND or HFD (Figure S3C). To further probe this previously-unrecognized function of dTMEM214 on glucose metabolism regulation, we utilized the *dTMEM-Gal4* driver to knock down *dTMEM214* (by over 60%; Figure 1E) in its endogenous expression sites followed by analysis of glucose metabolism in the knockdown flies (*dTMEM214-Gal4>dTMEM214*^{RNAi}). Compared to the *UAS-dTMEM214*^{RNAi} transgene or *dTMEM214-Gal4* driver control flies, the *dTMEM214-Gal4>dTMEM214*^{RNAi} flies displayed significantly reduced systemic glucose (Figure 1F) under ND and HSD. In insects,

trehalose is the dominant circulating sugar that is mainly derived from trehalose synthesized from glycogen in the fat body (Becker et al., 1996; Wegener et al., 2003). We therefore examined trehalose and its sources and found that hemolymph trehalose level (Figure 1G), fat body trehalose content (Figure 1H), and fat body glycogen level (Figure 1I) were all diminished in the *dTMEM214-Gal4>dTMEM214*^{RNAi} flies compared to control flies on ND and HSD. In sum, our results support a role for dTMEM214 in the maintenance of normal glucose homeostasis.

dTmem214 resides in the apical membrane and cytoplasm of the midgut enterocyte

To identify the tissue-specific action of dTMEM214 on glucose homeostasis control, we first determined the endogenous expression of dTMEM214 in various tissues by crossing the *dTMEM214-Gal4* line to a *UAS-GFP* reporter line. We detected GFP expression in several tissues including the salivary gland (Figures 2A-2A'), fat body (Figures 2B-2B'), and the midgut (Figures 2C-2C'). The midgut is an important site of nutrient absorption and regulator of systemic glucose homeostasis. We therefore further study the expression of dTMEM214 in the midgut by generating a dTMEM214 polyclonal antibody using a peptide that corresponds to the N-terminal amino acids of dTMEM214 (see also Materials and Methods). The specificity of the dTMEM214 antibody was validated by the following immunostaining experiments. First, the dTMEM214 immunoreactivity in the apical membrane (arrowheads, Figure 2D) or cytoplasm (asterisk, Figure 2D) of the w^{1118} midgut enterocytes was strongly diminished upon the pre-absorption of the antibody with the dTMEM214 antigen (Figure 2D'), Second, the antibody detected a heightened amount of dTmem214 (~40% greater) in the enterocyte apical surfaces of the *dTMEM214-Gal4>dTMEM21*$^{+}$ flies than in control *dTMEM214-Gal4* flies (Figure S4A-S4B', S4D). Reciprocally, a decreased amount of dTmem214 (>50% less) in the enterocyte apical surfaces of the *dTMEM214-Gal4>dTMEM214*^{RNAi} flies than in control *dTMEM214-Gal4* flies was detected by the antibody (Figure S4A-S4A', S4C-S4C'; S4D). To further define the expression pattern of dTMEM214 in the enterocyte apical membrane, we co-stained w^{1118} midguts with both the dTMEM214 and Myosin VIIA (Myo7a) antibodies and observed a gap between the dTMEM214 and Myo7a immunosignals in the apical membrane of the enterocytes (Figures 2E). As Myo7a is enriched in the base of the microvilli in the enterocyte apical membrane (Glowinski et al., 2014), our results suggest that dTMEM214 localizes to the microvillar tips of the enterocyte apical membrane (schematic inset; Figure 2E').

dTMEM214 functions in the midgut to regulate systemic glucose homeostasis

To interrogate whether dTMEM214 acts in the midgut to control systemic glucose homeostasis, we knocked down *dTMEM214* specifically in the midgut with two different midgut-specific drivers, *Caudal-Gal4* or *Myo1A-Gal4*, which led to the depletion of ~45% or ~70% of *dTMEM214* expression, respectively, in the midgut (Figures 3A-3B). Of note, both *Caudal-Gal4* and *Myo1A-Gal4* drivers are active in the enterocytes of the midgut (Buchon et al., 2013; Choi et al., 2008; Jiang and Edgar, 2009; Morgan et al., 1995). We observed that the targeted knockdown of *dTMEM214* with either driver was associated with a significant reduction in systemic glucose levels relative to the driver or *RNAi* transgene control flies (Figures 3C-3D). Moreover, circulating trehalose levels

were significantly decreased in the *Caudal-Gal4* and *Myo1A-Gal4*-directed *dTMEM214*-knockdown flies compared to the respective control flies (Figures 3E-3F). In addition, we detected significant decreases in fat body trehalose and glycogen levels in the *Caudal-Gal4*-directed dTMEM214-knockdown flies compared to control flies (Figures 3G-3H). Overall, the enterocyte-specific inhibition of dTMEM214 phenocopies the *dTMEM214-Gal4*-mediated inhibition of dTMEM214 (Figure 1), indicating an important role of dTMEM214 in the midgut in regulating systemic glucose homeostasis.

dTMEM214 mediates glucose uptake in the midgut

Based on our observations that dTMEM214 functions in the enterocytes to regulate systemic glucose homeostasis (Figures 2-3) and resides in the enterocyte surface membrane (Figures 2C-2C'), we posit that dTMEM214 is involved in dietary glucose uptake in the midgut. If that is the case, we further reasoned that loss of dTMEM214 would perturb glucose levels in the midgut. Indeed, significantly lower glucose levels were detected in the midguts of the *Caudal-Gal4* and *Myo1A-Gal4*-directed *dTMEM214*-knocked down flies compared to the respective control flies under ND and HSD (Figures 4A-4B). To directly assess the function of dTMEM214 in glucose uptake in the midgut, we utilized 2-(N-(7-Nitrobenz-2-oxa-1,3-diazol-4-yl)Amino)-2-Deoxyglucose (2-NBDG), a non-metabolizable fluorescent D-glucose analog, as an indicator of glucose uptake. 2-NBDG uptake in the midgut enterocytes has previously been shown to be blocked by glucose in a dose-dependent manner (Li et al., 2021), suggesting that 2-NBDG uptake accurately reflects glucose uptake in the midgut. Utilizing 2-NBDG in an ex vivo assay (whereby 2-NBDG was applied exogenously to freshly-dissected midguts; see Materials and Methods), we detected an obvious decrease in 2-NBDG uptake in the *Caudal-* or *Myo1A-Gal4*–directed *dTMEM214*-silenced midgut compared to the *RNAi* transgene control midguts under ND (Figures 4C-4E). Our quantification studies further revealed a significant and close to 40% reduction in 2-NBDG fluorescence in the enterocytes of the *Caudal-Gal4*– or *Myo1A-Gal4*– mediated dTMEM214-silenced midguts compared to control midguts (Figure 4F). In corroboration of the ex vivo assay results, we observed a similar decrease in 2-NBDG fluorescence levels in the enterocytes of the *Caudal-Gal4*– or *Myo1A-Gal4*–mediated *dTMEM214*-knockdown flies compared to that in control midguts upon their feeding of 2-NBDG on ND (in vivo assay; Figures 4G-4I). Upon quantification, we found that 2-NBDG fluorescence reached only ~45% (for *Caudal-Gal4*–mediated *dTMEM214*-knockdown midguts) and ~55% (for *Myo1A-Gal4*–mediated *dTMEM214*-knockdown midguts) of that in the control midgut (Figure 4J). We also examined the uptake of 2-NBDG in the midgut of a *dTMEM214* mutant strain and detected its lower level compared to that in the w^{1118} flies (Figures 4K-4L), by up to a significant 36% decrease (Figure 4M). Hence, we demonstrate that dTMEM214 regulates systemic glucose metabolism through, at least in part, by controlling glucose absorption in the midgut.

Rab4 acts in the midgut to regulate enterocyte glucose uptake and whole-body glucose homeostasis

The immunostaining pattern of dTMEM214 revealing its localization in both the apical membrane and cytoplasm of the enterocyte (Figure 2E) suggests that dTMEM214 undergoes dynamic cellular trafficking. Several Rab proteins (Rab 4, Rab5, and Rab 11) have been

shown to participate in the control of glucose transporter trafficking in insulin-responsive cells (Cormont and Le Marchand-Brustel, 2001) although their role in regulating the intracellular trafficking of glucose transporter in the small intestine has not been studied yet. As a first step towards understanding their potential role in glucose transport in the small intestine, we probed whether inhibition of several Rab proteins in the fly midgut might alter systemic glucose homeostasis. We found that silencing of *Rab4* or *Rab11* in the midgut significantly decreased systemic glucose levels on ND and HSD (Figures S5A and S5D), whereas silencing of *Rab7* in the midgut significantly increased systemic glucose levels on either diet (Figure S5C). The midgut-specific inhibition of Rab5, on the other hand, did not elicit any detectable changes on systemic glucose levels on ND or HSD (Figure S5B). Rab4 has been shown to play a key role in controlling glucose transporter intracellular trafficking in the insulin-responsive adipocytes and muscle cells (Aledo et al., 1995; Cormont et al., 1996; Mari et al., 2006; Ricort et al., 1994; Shibata et al., 1997). We therefore further examined whether Rab4 might regulate systemic glucose homeostasis through the control of glucose absorption in the midgut. Two lines of evidences support this notion, as shown in Figure 5. First, the midgut-specific knockdown of *Rab4* significantly lowered midgut glucose quantities on ND or HSD (Figure 5A). Second, the midgut-specific knockdown of *Rab4* strongly abolished the uptake of glucose in the enterocytes, as reflected by significantly decreased 2-NBDG fluorescence in the *Myo1A-Gal4*–mediated Rab4-silenced midguts (*Myo1A-Gal4>Rab4*^{RNAi}) compared to control midguts (*UAS- Rab4*^{RNAi}) in both ex vivo (Figures 5B-5D) and in vivo (Figures 5E-5G) assays. We conclude that Rab4, like dTMEM214, functions in the midgut to regulate glucose absorption.

Rab4 co-localizes with and regulates the subcellular distribution of dTMEM214 in enterocytes

Given their similar roles in governing enterocyte glucose absorption and systemic glucose homeostasis, we next determined whether Rab4 regulates dTMEM214 subcellular distribution or vice versa. First, we evaluated the expression pattern of Rab4 in the midgut enterocyte by overexpressing a Rab4-membrane red fluorescent protein (Rab4-mRFP) fusion protein in the midgut using the *Myo1A-Gal4* driver. It has been shown that in the *Drosophila* larval nervous system, the Rab4-mRFP signal strongly co-localizes with endogenous Rab4 identified using a Rab4 antibody whose epitope sequence is conserved in *Drosophila* (White et al., 2020). Moreover, it has been reported that ectopically expressed Rab4-mRFP co-localized with endogenously expressed YFP-Rab4 (protein trap) in the cell body and axons of lateral chordotonal neurons (Dey et al., 2017), Therefore, these results indicate that that Rab4-mRFP recapitulates endogenous Rab4 localization and trafficking. As shown in Figure 6A, we detected RFP expression in the cytoplasm of the *Myo1A-Gal4*–mediated *Rab4-mRFP* overexpressing enterocytes. Notably, when immunostained for dTMEM214 (Figure 6B), the *Myo1A-Gal4*–mediated *Rab4-mRFP* overexpressing enterocytes exhibited an obvious co-localization between the RFP fluorescence and the dTMEM214 immunosignal in the cytoplasm (Figures 6C-6C’). Based on these observations, we further assessed whether Rab4 regulates the proper subcellular localization of dTMEM214 in the enterocytes. To this end, we have examined the subcellular distribution of dTMEM214 in the *Myo1A-Gal4*–mediated Rab4-silenced enterocytes and observed a striking re-distribution of dTMEM214. A cross-sectional view of

the *Myo1A-Gal4>Rab4^{RNAi}* midgut found a diminution of dTMEM214 levels in the apical membranes of the enterocytes compared to the *UAS-Rab4^{RNAi}* control enterocytes (Figures 6D-6D'). This observation was reflected in the sagittal (longitudinal) view revealing a detectable decrease in the localization of dTMEM214 in the apical membrane accompanied by an increased accumulation of dTMEM214 in the cytoplasm of the enterocytes (Figures 6E-6E'). In contrast, the depletion of dTMEM214 does not significantly perturb Rab4, as the Rab4-RFP fluorescence level was comparable between the *Myo1A-Gal4*–mediated *dTMEM214*-silenced enterocytes and control enterocytes (Figures 6F-6F'). Together, these results indicate that Rab4 is required for the proper localization of dTMEM214 in the apical membrane, which could be important in the ability of dTMEM214 in regulating glucose uptake.

dTMEM214 co-localizes with dSLC5A5 and regulates the proper subcellular localization of dSLC5A5 in the midgut enterocytes

Previously we have demonstrated that *Drosophila* solute carrier 5A5 (dSLC5A5) mediates glucose uptake in the fly midgut enterocytes (Li et al., 2021). Further, we observed that dSLC5A5 resides in both the apical membrane and cytoplasm of the enterocyte [Figures 7A-7A'; (Li et al., 2021)] Given that both dTMEM214 and dSLC5A5 exhibit a similar apical membrane/cytoplasmic distribution profile in the enterocyte (Figures 7A-7B'), we assessed whether they could co-localize in the enterocyte. To address that, we performed co-immunostainings of midguts that overexpress dSLC5A5-FLAG driven by either *Myo1A-Gal4* (Figure S6) or the ubiquitous *Hsp70-Gal4* (Figure S7) using both the dTMEM214 antibody and FLAG antibodies. Under the cross-sectional view, we observed substantial co-localizations of the dTMEM214 and FLAG immunoreactivities in the apical membrane (Figures S6A-S6A"; S7A-S7A") and cytoplasm (Figures S6B-S6B"; S7B-S7B") of the enterocytes. Under the sagittal view, we similarly detected strong co-localizations of the dTMEM214 and FLAG immunoreactivities in the apical membrane and cytoplasm of the enterocytes (Figures S6C-S6C"; S7C-S7C").

In light of their co-localization, we further asked if dTMEM214 might control subcellular distribution of dSLC5A5 in the enterocytes. If that is the case, we postulated that altering the levels of dTMEM214 would perturb the normal distribution of dSLC5A5 between the surface membrane and cytoplasm in the enterocytes. Indeed, in the dTMEM214-silenced enterocytes that concomitantly overexpressed dSLC5A5-FLAG directed by either *Caudal-Gal4 (Caudal-Gal4>dTMEM214^{RNAi};dSLC5A5-FLAG*) or *Myo1A-Gal4 (MyoIA-Gal4>dTMEM214 ^{RNAi};dSLC5A5-FLAG*), we observed that the levels of dSLC5A5 (marked by FLAG immunoreactivity; Figures 7B-7B' and 7H-7H') were diminished in the apical membrane (marked by F-actin, Figures 7B' and 7H') compared to the control dSLC5A5-FLAG-overexpressing enterocytes (Figures 7A-7A' and 7G-7G'). Concomitantly, there was an increase in the cytoplasmic level of dSLC5A5 in the *Caudal-Gal4>dTMEM214^{RNAi};dSLC5A5-FLAG* enterocytes (Figures 7D-7D') or *MyoIA-Gal4>dTMEM214^{RNAi};dSLC5A5-FLAG* enterocytes (Figures 7J-7J') compared to their respective control dSLC5A5-FLAG–overexpressing enterocytes (Figures 7C-7C', 7I-7I'). In addition, a sagittal view also revealed a redistribution of dSLC5A5 from the apical membrane (marked by F-actin) to the cytoplasm in the

Caudal-Gal4>dTMEM214^{RNAi};dSLC5A5-FLAG enterocytes (Figures 7F-7F) or *MyoIA-Gal4>dTMEM214^{RNAi};dSLC5A5-FLAG* enterocytes (Figures 7L-7L') compared to their respective dSLC5A5-FLAG–overexpressing enterocytes (Figures 7E-7E', 7K-7K'). In contrast, the knockdown (Figure S8) or overexpression (Figure S9) of *dSLC5A5* in the midgut driven by *Caudal-Gal4* did not elicit any detectable alterations in the levels of dTMEM214 in either the apical membrane (Figures S7B-S7B', S7C, S9B-S9B', S9C) or cytoplasm (Figures S8E-S8E', S8F, S9E-S9E', S9F) compared to the *UAS-dSLC5A5^{RNAi}* control enterocytes (Figures S8A-S8A', S8D-S8D', S8C, S8F) or *UAS-dSLC5A5-FLAG* control enterocytes (Figures S9A-S9A', S9D-S9D', S9C, S9F), respectively. In agreement with the above observations, a sagittal view similarly showed that the dTMEM214 subcellular distribution in the apical membrane and cytoplasm of the *Caudal-Gal4>dSLC5A5^{RNAi}* (Figures S8H-S8H', S8I-S8J) or *Caudal-Gal4>dSLC5A5-FLAG* (Figures S9H-S9H', S9I-S9J) enterocytes remained comparable to that in the *UAS-dSLC5A5^{RNAi}* (Figures S8G-S8G', S8I-S8J) or *UAS-dSLC5A5-FLAG* (Figures S9G-S9G', S9I-S9J) control enterocytes, respectively. These results indicate that dTMEM214 regulates the normal subcellular localization of dSLC5A5 in the enterocyte.

Discussion

In this study, we reveal new regulators of the subcellular distribution of the glucose transporter in the *Drosophila* midgut enterocyte. From a genetic screen, we identified that dTMEM214 plays an important role in modulating systemic glucose homeostasis, by controlling glucose absorption in the enterocyte. We show that dTMEM214 localizes to the apical membrane and cytoplasm of the enterocyte, and that the subcellular distribution of dTMEM214 in the enterocyte is controlled by Rab4. As a corollary, the midgut-specific knockdown of Rab4 perturbs normal systemic glucose homeostasis and inhibits glucose uptake in the enterocyte similarly to that seen with the knockdown of *dTMEM214* in the midgut. In further interrogation of the mechanism of action of dTMEM214 on glucose homeostasis modulation, we found that dTMEM214 regulates the proper subcellular localization of dSLC5A5, a protein recently identified to mediate glucose uptake in the midgut enterocyte (Li et al., 2021).

So far, our knowledge of the biological functions of TMEM214 remains limited. TMEM214 has been linked to ER stress-mediated apoptosis in a cultured cell study (Li et al., 2013), to human mRNA decay in yeast two-hybrid screening (Lehner and Sanderson, 2004), and to survival under hyperoxia in *Drosophila* genetic screening (Zhao et al., 2010). Our study here shows for the first time that dTMEM214 regulates systemic glucose homeostasis, further highlighting the versatility of TMEM214 function. Moreover, unpublished work in our lab has found that dTMEM214 is a single-pass transmembrane protein that shares between 25 to 31 percent identity to orthologs in human, dog, rabbit, mouse, chicken, frog, and zebrafish. Interestingly, we further identified several common LC3-interacting region (LIR) motifs within the N-terminal domains of the human, rat, mouse and *Drosophila* TMEM214. As the LIR motifs are known to be critical for interacting with the LC3 receptor on the autophagosomes (Johansen and Lamark, 2020), our findings suggest that TMEM214 might serve as an adaptor to direct its interacting proteins to the autophagosome for their degradation via autophagy. This possibility remains to be interrogated.

Previous work had reported that TMEM214 is present in the nuclear envelope and the ER in cultured cells (Wilkie et al., 2011). Our work here further shows that dTMEM214 resides in the surface membrane and cytoplasmic vesicles in the midgut enterocyte. The multiple cellular localizations of TMEM214 led us to propose that dTMEM214 undergoes vesicular trafficking from the intracellular organelles to the apical membrane in the *Drosophila* enterocyte. Interestingly, we found that dTMEM214 co-localizes with Rab4 amongst the cytoplasmic vesicles in the enterocyte. Rab4 is localized to early endocytic compartments (sorting and recycling endosomes) and regulates recycling from early endosomes back to the plasma membrane (de Wit et al., 1999; de Wit et al., 2001; Roberts et al., 2001; van der Sluijs et al., 1992a). It is therefore conceivable that dTMEM214 in the enterocyte undergoes apical endocytosis into the Rab4-containing early endosomes and gets recycled back to the apical membrane in a Rab4-dependent manner. In support of this notion, we observed a depletion of dTMEM214 in the apical membrane and a concomitant build-up of dTMEM214 in the cytoplasm of the *Rab4*-silenced enterocytes, whereby recycling to the apical membrane is anticipated to be perturbed.

Our study further found that in the *dTMEM214*-silenced enterocytes, dSLC5A5 was similarly redistributed from the surface membrane to the cytoplasmic pool of vesicular puncta, raising the possibility that dTMEM214 regulates the trafficking of dSLC5A5 to the apical membrane. dSLC5A5 was previously shown to undergo apical endocytosis in the enterocyte and may be recycled back to the apical membrane or targeted for lysosomal degradation following its endocytosis (Li et al., 2021). Two scenarios can be envisioned by which dTMEM214 underlies the apical localization of dSLC5A5 in the enterocyte. First, dTMEM214 regulates the stability of dSLC5A5 in the apical membrane. In the absence of dTMEM214, dSLC5A5 might undergo apical endocytosis at a higher rate that results in its surface membrane depletion. Second, dTMEM214 promotes the recycling of dSLC5A5 back to the surface membrane upon the apical endocytosis of dSLC5A5. In the absence of dTMEM214, recycling of dSLC5A5 to the surface membrane might be blunted, resulting in its apical depletion. Future work remains to distinguish between these two scenarios, which entails the monitoring of dSLC5A5 in the dTMEM214-depleted or overexpressing enterocytes by labeling with a dSLC5A5 specific antibody, which is currently lacking.

In summary, our present work identifies new molecular players important in regulating the apical targeting of glucose transporter in the *Drosophila* enterocyte, which may provide insights into the normal subcellular distribution of SGLT1 in the small intestine that is pertinent to the maintenance of normal systemic glucose homeostasis.

Supplementary Material

Refer to Web version on PubMed Central for supplementary material.

Acknowledgments

We thank our colleagues for thoughtful comments on the manuscript. We thank the Bloomington *Drosophila* stock center and the Vienna *Drosophila* RNAi Center for fly stocks. We thank the Cell Biology Imaging Core Facility at OUHSC for technical assistance on confocal microscopy. H.-Y.L. and W.W. conceived and designed the research; Y.L. and H.-Y.L. performed the research and acquired the data; H.-Y.L. and W.W. analyzed and interpreted the data. H.-Y.L. and W.W. drafted and revised the manuscript.

Funding sources

This work was supported by grants from the NIH (5R01HL152205 to H.-Y.L. and 5R01DK116017 and 5R01DK128848 to W.W.).

Data Availability Statement

The data that support the findings of this study are available in the methods and/or supplementary material of this article.

References

Aledo JC, Darakhshan F, Hundal HS, 1995. Rab4, but not the transferrin receptor, is colocalized with GLUT4 in an insulin-sensitive intracellular compartment in rat skeletal muscle. Biochem Biophys Res Commun 215, 321–328. [PubMed: 7575609]

Barbero P, Bittova L, Pfeffer SR, 2002. Visualization of Rab9-mediated vesicle transport from endosomes to the trans-Golgi in living cells. J Cell Biol 156, 511–518. [PubMed: 11827983]

Becker A, Schloder P, Steele JE, Wegener G, 1996. The regulation of trehalose metabolism in insects. Experientia 52, 433–439. [PubMed: 8706810]

Buchon N, Osman D, David FP, Fang HY, Boquete JP, Deplancke B, Lemaitre B, 2013. Morphological and molecular characterization of adult midgut compartmentalization in Drosophila. Cell Rep 3, 1725–1738. [PubMed: 23643535]

Carroll KS, Hanna J, Simon I, Krise J, Barbero P, Pfeffer SR, 2001. Role of Rab9 GTPase in facilitating receptor recruitment by TIP47. Science 292, 1373–1376. [PubMed: 11359012]

Casavola EC, Catucci A, Bielli P, Di Pentima A, Porcu G, Pennestri M, Cicero DO, Ragnini-Wilson A, 2008. Ypt32p and Mlc1p bind within the vesicle binding region of the class V myosin Myo2p globular tail domain. Mol Microbiol 67, 1051–1066. [PubMed: 18221262]

Chan CC, Scoggin S, Wang D, Cherry S, Dembo T, Greenberg B, Jin EJ, Kuey C, Lopez A, Mehta SQ, Perkins TJ, Brankatschk M, Rothenfluh A, Buszczak M, Hiesinger PR, 2011. Systematic discovery of Rab GTPases with synaptic functions in Drosophila. Curr Biol 21, 1704–1715. [PubMed: 22000105]

Choi YJ, Hwang MS, Park JS, Bae SK, Kim YS, Yoo MA, 2008. Age-related upregulation of Drosophila caudal gene via NF-kappaB in the adult posterior midgut. Biochim Biophys Acta 1780, 1093–1100. [PubMed: 18656526]

Cobbold C, Monaco AP, Sivaprasadarao A, Ponnambalam S, 2003. Aberrant trafficking of transmembrane proteins in human disease. Trends Cell Biol 13, 639–647. [PubMed: 14624842]

Cormont M, Bortoluzzi MN, Gautier N, Mari M, van Obberghen E, Le Marchand-Brustel Y, 1996. Potential role of Rab4 in the regulation of subcellular localization of Glut4 in adipocytes. Mol Cell Biol 16, 6879–6886. [PubMed: 8943343]

Cormont M, Le Marchand-Brustel Y, 2001. The role of small G-proteins in the regulation of glucose transport (review). Mol Membr Biol 18, 213–220. [PubMed: 11681788]

Cormont M, Mari M, Galmiche A, Hofman P, Le Marchand-Brustel Y, 2001. A FYVE-finger-containing protein, Rabip4, is a Rab4 effector involved in early endosomal traffic. Proc Natl Acad Sci U S A 98, 1637–1642. [PubMed: 11172003]

de Wit H, Lichtenstein Y, Geuze HJ, Kelly RB, van der Sluijs P, Klumperman J, 1999. Synaptic vesicles form by budding from tubular extensions of sorting endosomes in PC12 cells. Mol Biol Cell 10, 4163–4176. [PubMed: 10588650]

de Wit H, Lichtenstein Y, Kelly RB, Geuze HJ, Klumperman J, van der Sluijs P, 2001. Rab4 regulates formation of synaptic-like microvesicles from early endosomes in PC12 cells. Mol Biol Cell 12, 3703–3715. [PubMed: 11694600]

Dey S, Banker G, Ray K, 2017. Anterograde Transport of Rab4-Associated Vesicles Regulates Synapse Organization in Drosophila. Cell Rep 18, 2452–2463. [PubMed: 28273459]

Dunst S, Kazimiers T, von Zadow F, Jambor H, Sagner A, Brankatschk B, Mahmoud A, Spannl S, Tomancak P, Eaton S, Brankatschk M, 2015. Endogenously tagged rab proteins: a resource to study membrane trafficking in Drosophila. Dev Cell 33, 351–365. [PubMed: 25942626]

Fouraux MA, Deneka M, Ivan V, van der Heijden A, Raymackers J, van Suylekom D, van Venrooij WJ, van der Sluijs P, Pruijn GJ, 2004. Rabip4' is an effector of rab5 and rab4 and regulates transport through early endosomes. Mol Biol Cell 15, 611–624. [PubMed: 14617813]

Gillingham AK, Sinka R, Torres IL, Lilley KS, Munro S, 2014. Toward a comprehensive map of the effectors of rab GTPases. Dev Cell 31, 358–373. [PubMed: 25453831]

Glowinski C, Liu RH, Chen X, Darabie A, Godt D, 2014. Myosin VIIA regulates microvillus morphogenesis and interacts with cadherin Cad99C in Drosophila oogenesis. J Cell Sci 127, 4821–4832. [PubMed: 25236597]

Grigoriev I, Splinter D, Keijzer N, Wulf PS, Demmers J, Ohtsuka T, Modesti M, Maly IV, Grosveld F, Hoogenraad CC, Akhmanova A, 2007. Rab6 regulates transport and targeting of exocytotic carriers. Dev Cell 13, 305–314. [PubMed: 17681140]

Grosshans BL, Andreeva A, Gangar A, Niessen S, Yates JR 3rd, Brennwald P, Novick P, 2006. The yeast lgl family member Sro7p is an effector of the secretory Rab GTPase Sec4p. J Cell Biol 172, 55–66. [PubMed: 16390997]

Hutagalung AH, Novick PJ, 2011. Role of Rab GTPases in membrane traffic and cell physiology. Physiol Rev 91, 119–149. [PubMed: 21248164]

Jiang H, Edgar BA, 2009. EGFR signaling regulates the proliferation of Drosophila adult midgut progenitors. Development 136, 483–493. [PubMed: 19141677]

Jin EJ, Chan CC, Agi E, Cherry S, Hanacik E, Buszczak M, Hiesinger PR, 2012. Similarities of Drosophila rab GTPases based on expression profiling: completion and analysis of the rab-Gal4 kit. Plos One 7, e40912. [PubMed: 22844416]

Johansen T, Lamark T, 2020. Selective Autophagy: ATG8 Family Proteins, LIR Motifs and Cargo Receptors. J Mol Biol 432, 80–103. [PubMed: 31310766]

Jordens I, Fernandez-Borja M, Marsman M, Dusseljee S, Janssen L, Calafat J, Janssen H, Wubbolts R, Neefjes J, 2001. The Rab7 effector protein RILP controls lysosomal transport by inducing the recruitment of dynein-dynactin motors. Curr Biol 11, 1680–1685. [PubMed: 11696325]

Kohrs FE, Daumann IM, Pavlovic B, Jin EJ, Kiral FR, Lin SC, Port F, Wolfenberg H, Mathejczyk TF, Linneweber GA, Chan CC, Boutros M, Hiesinger PR, 2021. Systematic functional analysis of rab GTPases reveals limits of neuronal robustness to environmental challenges in flies. Elife 10.

Lee JO, Lee SK, Jung JH, Kim JH, You GY, Kim SJ, Park SH, Uhm KO, Kim HS, 2011. Metformin induces Rab4 through AMPK and modulates GLUT4 translocation in skeletal muscle cells. J Cell Physiol 226, 974–981. [PubMed: 20857458]

Lehner B, Sanderson CM, 2004. A protein interaction framework for human mRNA degradation. Genome Res 14, 1315–1323. [PubMed: 15231747]

Li C, Wei J, Li Y, He X, Zhou Q, Yan J, Zhang J, Liu Y, Liu Y, Shu HB, 2013. Transmembrane Protein 214 (TMEM214) mediates endoplasmic reticulum stress-induced caspase 4 enzyme activation and apoptosis. J Biol Chem 288, 17908–17917. [PubMed: 23661706]

Li L, Omata W, Kojima I, Shibata H, 2001. Direct interaction of Rab4 with syntaxin 4. J Biol Chem 276, 5265–5273. [PubMed: 11063739]

Li Y, Wang W, Lim HY, 2021. Drosophila Solute Carrier 5A5 Regulates Systemic Glucose Homeostasis by Mediating Glucose Absorption in the Midgut. Int J Mol Sci 22.

Liu Y, Bao H, Wang W, Lim HY, 2019. Cardiac Snail family of transcription factors directs systemic lipid metabolism in Drosophila. PLoS Genet 15, e1008487. [PubMed: 31725726]

Mari M, Monzo P, Kaddai V, Keslair F, Gonzalez T, Le Marchand-Brustel Y, Cormont M, 2006. The Rab4 effector Rabip4 plays a role in the endocytotic trafficking of Glut 4 in 3T3-L1 adipocytes. J Cell Sci 119, 1297–1306. [PubMed: 16522682]

Morgan NS, Heintzelman MB, Mooseker MS, 1995. Characterization of myosin-IA and myosin-IB, two unconventional myosins associated with the Drosophila brush border cytoskeleton. Dev Biol 172, 51–71. [PubMed: 7589814]

Nielsen E, Christoforidis S, Uttenweiler-Joseph S, Miaczynska M, Dewitte F, Wilm M, Hoflack B, Zerial M, 2000. Rabenosyn-5, a novel Rab5 effector, is complexed with hVPS45 and recruited to endosomes through a FYVE finger domain. J Cell Biol 151, 601–612. [PubMed: 11062261]

Pundir S, Martin MJ, O'Donovan C, 2017. UniProt Protein Knowledgebase. Methods Mol Biol 1558, 41–55. [PubMed: 28150232]

Reiter LT, Potocki L, Chien S, Gribskov M, Bier E, 2001. A systematic analysis of human disease-associated gene sequences in Drosophila melanogaster. Genome Res 11, 1114–1125. [PubMed: 11381037]

Ricort JM, Tanti JF, Cormont M, Van Obberghen E, Le Marchand-Brustel Y, 1994. Parallel changes in Glut 4 and Rab4 movements in two insulin-resistant states. FEBS Lett 347, 42–44. [PubMed: 8013658]

Roberts M, Barry S, Woods A, van der Sluijs P, Norman J, 2001. PDGF-regulated rab4-dependent recycling of alphavbeta3 integrin from early endosomes is necessary for cell adhesion and spreading. Curr Biol 11, 1392–1402. [PubMed: 11566097]

Roder PV, Geillinger KE, Zietek TS, Thorens B, Koepsell H, Daniel H, 2014. The Role of SGLT1 and GLUT2 in Intestinal Glucose Transport and Sensing. Plos One 9.

Rojas R, van Vlijmen T, Mardones GA, Prabhu Y, Rojas AL, Mohammed S, Heck AJ, Raposo G, van der Sluijs P, Bonifacino JS, 2008. Regulation of retromer recruitment to endosomes by sequential action of Rab5 and Rab7. J Cell Biol 183, 513–526. [PubMed: 18981234]

Sato T, Mushiake S, Kato Y, Sato K, Sato M, Takeda N, Ozono K, Miki K, Kubo Y, Tsuji A, Harada R, Harada A, 2007. The Rab8 GTPase regulates apical protein localization in intestinal cells. Nature 448, 366–369. [PubMed: 17597763]

Schmit K, Michiels C, 2018. TMEM Proteins in Cancer: A Review. Front Pharmacol 9, 1345. [PubMed: 30574087]

Sedzikowska A, Szablewski L, 2021. Human Glucose Transporters in Renal Glucose Homeostasis. Int J Mol Sci 22.

Shibata H, Omata W, Kojima I, 1997. Insulin stimulates guanine nucleotide exchange on Rab4 via a wortmannin-sensitive signaling pathway in rat adipocytes. J Biol Chem 272, 14542–14546. [PubMed: 9169411]

Strom M, Hume AN, Tarafder AK, Barkagianni E, Seabra MC, 2002. A family of Rab27-binding proteins. Melanophilin links Rab27a and myosin Va function in melanosome transport. J Biol Chem 277, 25423–25430. [PubMed: 11980908]

van der Sluijs P, Hull M, Huber LA, Male P, Goud B, Mellman I, 1992a. Reversible phosphorylation--dephosphorylation determines the localization of rab4 during the cell cycle. EMBO J 11, 4379–4389. [PubMed: 1425574]

van der Sluijs P, Hull M, Webster P, Male P, Goud B, Mellman I, 1992b. The small GTP-binding protein rab4 controls an early sorting event on the endocytic pathway. Cell 70, 729–740. [PubMed: 1516131]

Wegener G, Tschiedel V, Schloder P, Ando O, 2003. The toxic and lethal effects of the trehalase inhibitor trehazolin in locusts are caused by hypoglycaemia. J Exp Biol 206, 1233–1240. [PubMed: 12604583]

White JA 2nd, Krzystek TJ, Hoffmar-Glennon H, Thant C, Zimmerman K, Iacobucci G, Vail J, Thurston L, Rahman S, Gunawardena S, 2020. Excess Rab4 rescues synaptic and behavioral dysfunction caused by defective HTT-Rab4 axonal transport in Huntington's disease. Acta Neuropathol Commun 8, 97. [PubMed: 32611447]

Wilkie GS, Korfali N, Swanson SK, Malik P, Srsen V, Batrakou DG, de las Heras J, Zuleger N, Kerr AR, Florens L, Schirmer EC, 2011. Several novel nuclear envelope transmembrane proteins identified in skeletal muscle have cytoskeletal associations. Mol Cell Proteomics 10, M110 003129.

Zhao HW, Zhou D, Nizet V, Haddad GG, 2010. Experimental selection for Drosophila survival in extremely high O2 environments. Plos One 5, e11701. [PubMed: 20668515]

Highlights

- dTMEM214 acts in the midgut enterocytes to regulate systemic glucose homeostasis.
- The subcellular distribution of dTMEM214 in the enterocytes is regulated by Rab4.
- dTMEM214 controls the apical membrane localization of dSLC5A5 in the enterocytes.

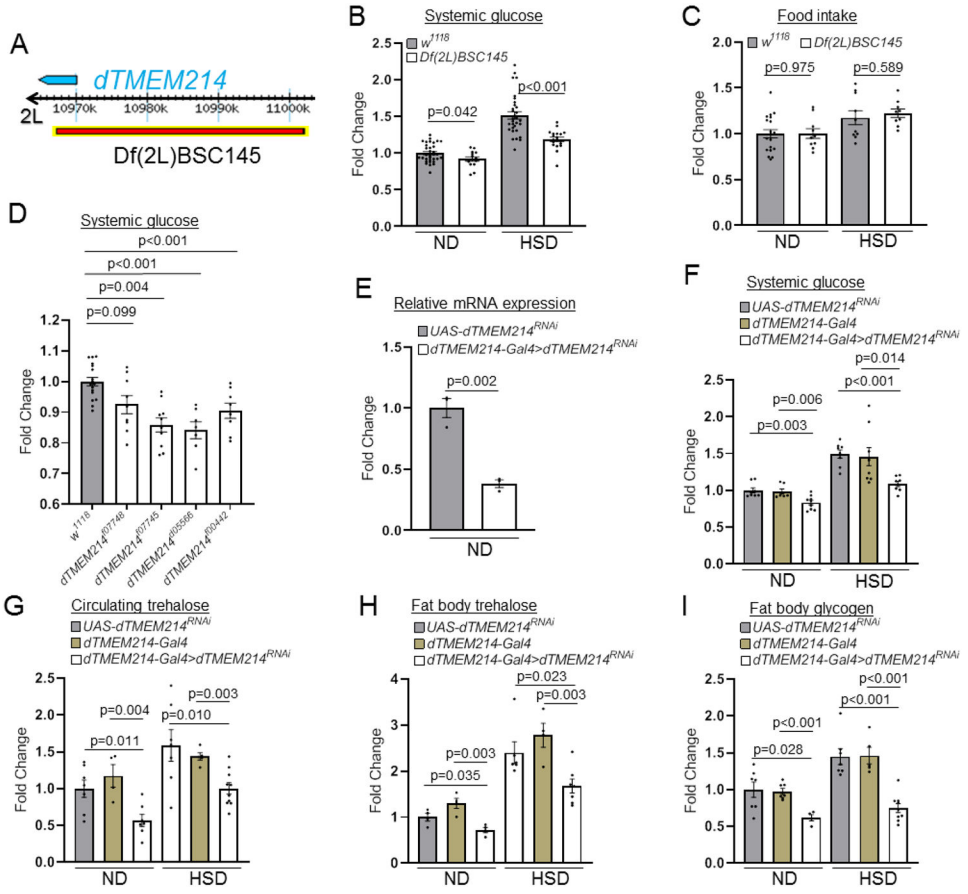

Figure 1. Whole-body knockdown of *dTMEM214* perturbs systemic glucose metabolism without affecting food intake.

(A) Schematic of the results of the genetic screen showing the location of the *dTMEM214* gene (blue symbol) on chromosome 2L. Red bar indicates the deletion in the *Df(2L)BSC145* deficiency line investigated in this study. (B) Systemic glucose levels in wide-type (w^{1118}) and *Df(2L)BSC145* on ND or HSD (N=15-30 dots/bar, n=120-240 flies, mean±SEM). Systemic glucose levels (μg/μl) were normalized to whole-body protein (μg/μl). (C) Food consumption in in wide-type (w^{1118}) and *Df(2L)BSC145* on ND or HSD (N=8-18 dots/bar, n=64-144 flies, mean±SEM). (D) Systemic glucose levels in different *dTMEM214* homozygous mutants (w^{1118}) on ND (N=8-17 dots/bar, n=64-140 flies, mean±SEM). Systemic glucose levels (μg/μl) were normalized to whole-body protein (μg/μl). (E) Quantitative real-time PCR analysis of the whole-fly levels of *dTMEM214* in transgene control flies (*UAS-dTMEM214*^{RNAi}) or in *dTMEM214*-knocked down flies by *dTMEM214-Gal4 driver (dTMEM214-Gal4>UAS-dTMEM214*^{RNAi}). (N=3 dots/bar, n=45 flies, mean±SEM). Relative expression of *dTMEM214* is set to 1 for the control. (F) Systemic glucose levels in transgene control flies (*UAS-dTMEM214*^{RNAi}*), Gal4* control flies (*dTMEM214-Gal4*) or in *dTMEM214*-knocked down flies by *dTMEM214-Gal4 driver (dTMEM214-Gal4>UAS-dTMEM214*^{RNAi}). Systemic glucose levels (μg/μl) were normalized to whole-body protein (μg/μl). (N=7-9 dots/bar, n=56-72 flies, mean±SEM). (G) Circulating levels of trehalose in transgene control flies (*UAS-dTMEM214*^{RNAi}*), Gal4* control flies (*dTMEM214-Gal4*) or in *dTMEM214*-knocked down flies by *dTMEM214-*

Gal4 driver (dTMEM214-Gal4>UAS-dTMEM214^{RNAi}). (N=5-9 dots/bar, n=175-315 flies, mean±SEM). (H-I) Fat body trehalose (H) or glycogen (I) content in transgene control flies (*UAS-dTMEM214^{RNAi}), Gal4* control flies (*dTMEM214-Gal4*) or in *dTMEM214*-knocked down flies by *dTMEM214-Gal4 driver (dTMEM214-Gal4>UAS-dTMEM214^{RNAi})*. (N=5-7 dots/bar, n=60-84 fat bodies, mean±SEM). Two-tailed Student's *t*-test was used to derive *p*-values between the *w^{1118}* and *dTMEM214* mutant flies, or between the transgene control and knockdown flies. ND, normal diet, HSD, high sugar diet.

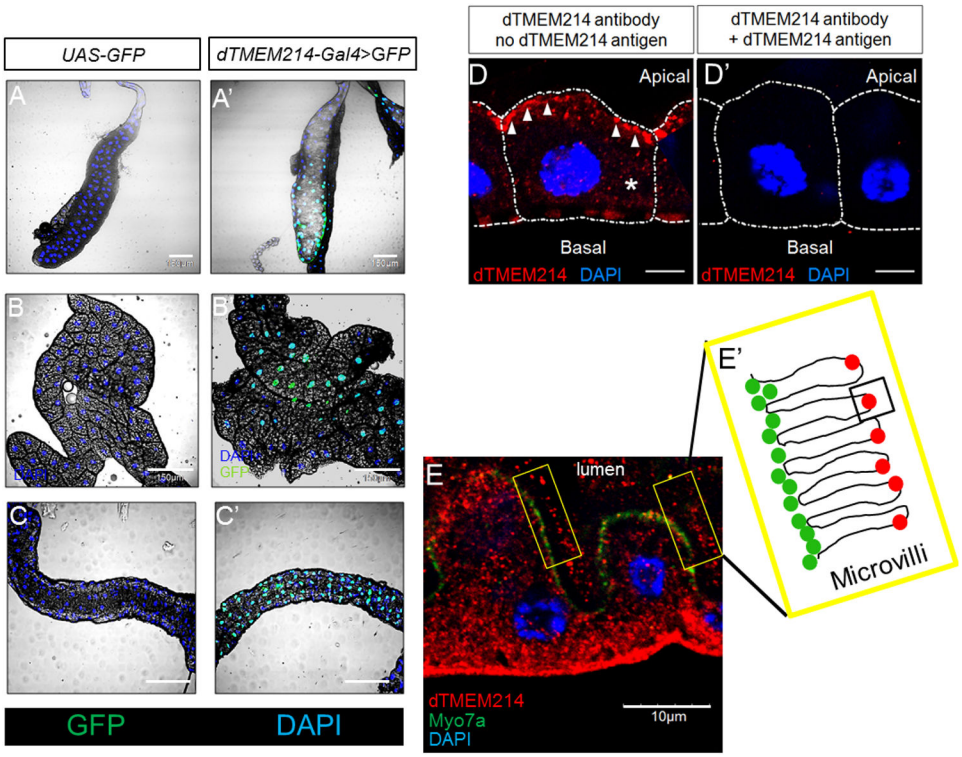

Figure 2. Whole-body knockdown of *dTMEM214* perturbs systemic glucose metabolism without affecting food intake.

(A-C') Representative confocal images of GFP (green) and DNA (blue) immunostainings in the salivary gland (A-A'), fat body (B-B'), and midgut (C-C') of the transgene control larvae (UAS-GFP) and *dTMEM214-Gal4*-mediated GFP-overexpressing larvae. Scale bar=150 μm. (D-D') Representative confocal images of dTMEM214 (red) and DNA (blue) immunostainings in wide-type enterocytes with dTMEM214 antibody alone (D) or with dTMEM214 antibody pre-absorbed with dTMEM214 antigen (D'). Scale bar=5 μm. (E) Representative confocal image of dTMEM214 (red), Myo7a (green) and DNA (blue) immunostainings in wide-type enterocytes incubated with dTMEM214 antibody. Scale bar=10 μm. (E') Schematic inset depicting the proposed residence of dTMEM214 (red) and Myo7a (green) in the apical membrane microvilli of the enterocyte denoted by yellow boxes in (E).

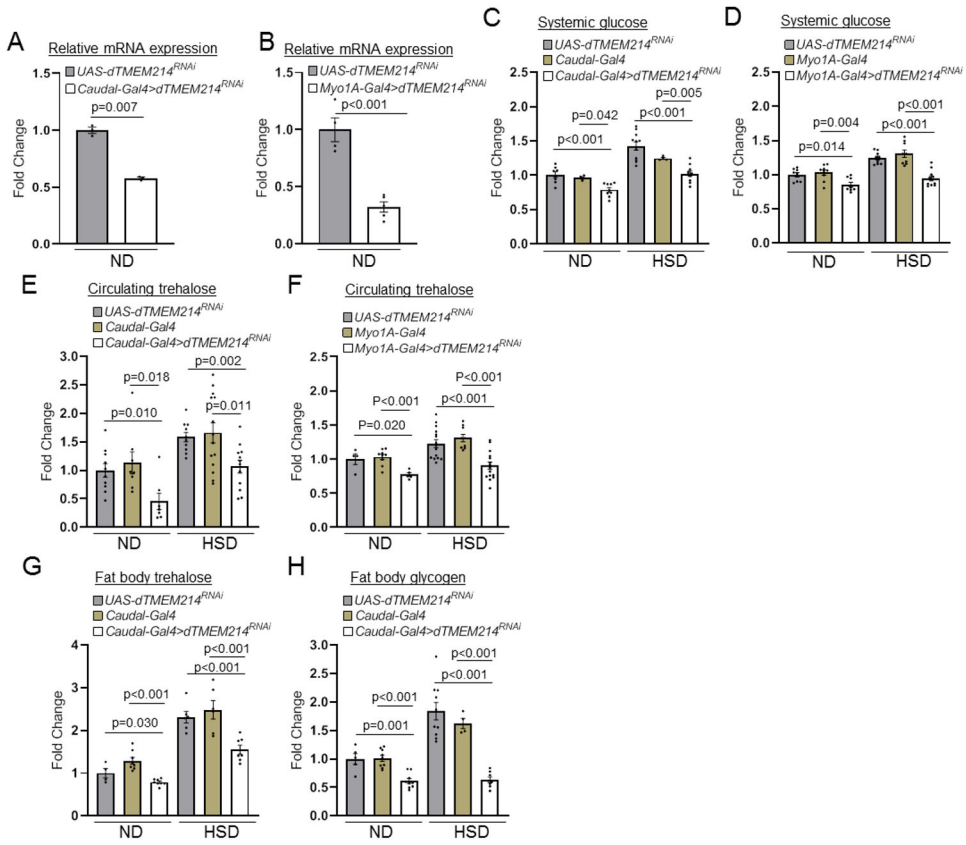

Figure 3. Midgut-specific knockdown of *dTMEM214* perturbs systemic glucose metabolism without affecting food intake.

(A-B) Quantitative real-time PCR analysis of the whole-fly levels of *dTMEM214* in transgene control flies (*UAS-dTMEM214^{RNAi}*) or in *dTMEM214*-knocked down flies by *Caudal-Gal4* driver (A) or *Myo1A-Gal4* (B). (N=3-5 dots/bar, n=45-75 flies, mean±SEM). (C-D) Systemic glucose levels in transgene control flies (*UAS-dTMEM214^{RNAi}), Gal4* control flies or in *dTMEM214*-knocked down flies by *Caudal-Gal4 driver* (C) or *Myo1A-Gal4* driver (D). Systemic glucose levels (μg/μl) were normalized to whole-body protein (μg/μl). (N=5-10 dots/bar, n=40-80 flies, mean±SEM). (E-F) Circulating levels of trehalose in transgene control flies (*UAS-dTMEM214^{RNAi}), Gal4* control flies or in *dTMEM214*-knocked down flies by *Caudal-Gal4 driver* (E) or *Myo1A-Gal4* driver (F). (N=5-15 dots/bar, n=175-525 flies, mean±SEM). (G-H) Fat body trehalose (G) or glycogen (H) content in transgene control flies (*UAS-dTMEM214^{RNAi}), Gal4* control flies (*Caudal-Gal4*) or in *dTMEM214*-knocked down flies by *Caudal-Gal4 driver (Caudal-Gal4>UAS-dTMEM214^{RNAi}*). (N=5-10 dots/bar, n=60-120 fat bodies, mean±SEM). Two-tailed Student's *t*-test was used to derive *p*-values between the transgene control and knockdown flies. ND, normal diet, HSD, high sugar diet.

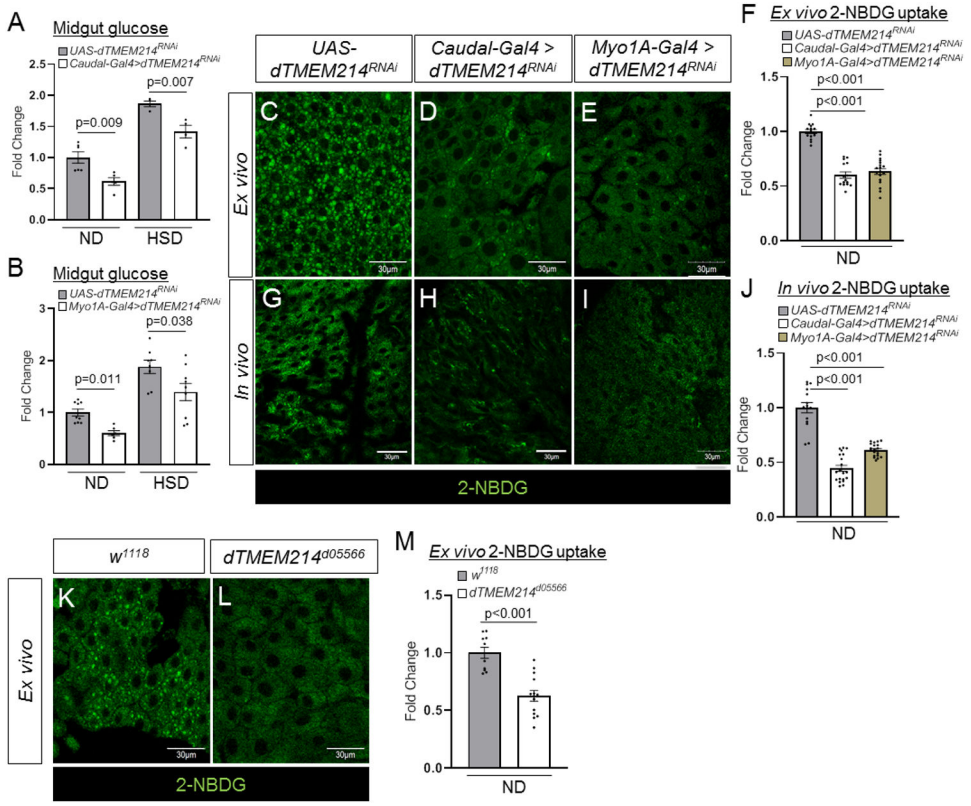

Figure 4. Inhibition of dTMEM214 disrupts glucose uptake in the enterocytes.

(A-B) Midgut glucose levels in transgene control (*UAS-dTMEM214*^{RNAi}) or in *dTMEM214*-knocked down flies by *Caudal-Gal4* (A) or *Myo1A-Gal4* (B). Midgut glucose levels (μg/μl) were normalized to total protein of midguts (μg/μl). (N=5-6 dots/bar, n=60-72 midguts, mean±SEM). Twelve midguts of each genotype were collected for each independent experiment. (C-E, G-I) Representative confocal images of the intracellular accumulation of 2-NBDG in the *ex-vivo* (C-E) or *in-vivo* (G-I) enterocytes of transgene control flies (*UAS-dTMEM214*^{RNAi}) (C, G) or in *dTMEM214*-knocked down flies by *Caudal-Gal4 driver* (D, H) or *Myo1A-Gal4* driver (E, I). Scale bars represent 30 μm. (F, J) Quantification of 2-NBDG fluorescence with the mean intensity for the different genotypes normalized to that of transgene control flies (*UAS-dTMEM214*^{RNAi}; set at 1.0) in *ex-vivo* enterocyte assay (F) or *in-vivo* enterocyte assay (J). (N=15-19 dots/bar, n=5-6 midguts with 2-3 different areas per midgut quantified, mean±SEM). The R4-R5 midgut region was quantified. (K-L) Representative confocal images of the intracellular accumulation of 2-NBDG in the enterocytes of wild-type flies (*w*^{1118}) (K) or *dTMEM214* mutant (*f05566*) (L). Scale bars represent 30 μm. (M) Quantification of 2-NBDG fluorescence with the mean intensity for the *dTMEM214* mutant (*f05566*) flies normalized to that of wild-type flies (*w*^{1118}; set at 1.0). (N=10-14 dots/bar, n=5-7 midguts with 2-3 different areas per midgut quantified, mean±SEM). The R4-R5 midgut region was quantified. Two-tailed Student's *t*-test was used to derive *p*-values between the transgene control and knockdown flies. ND, normal diet, HSD, high sugar diet.

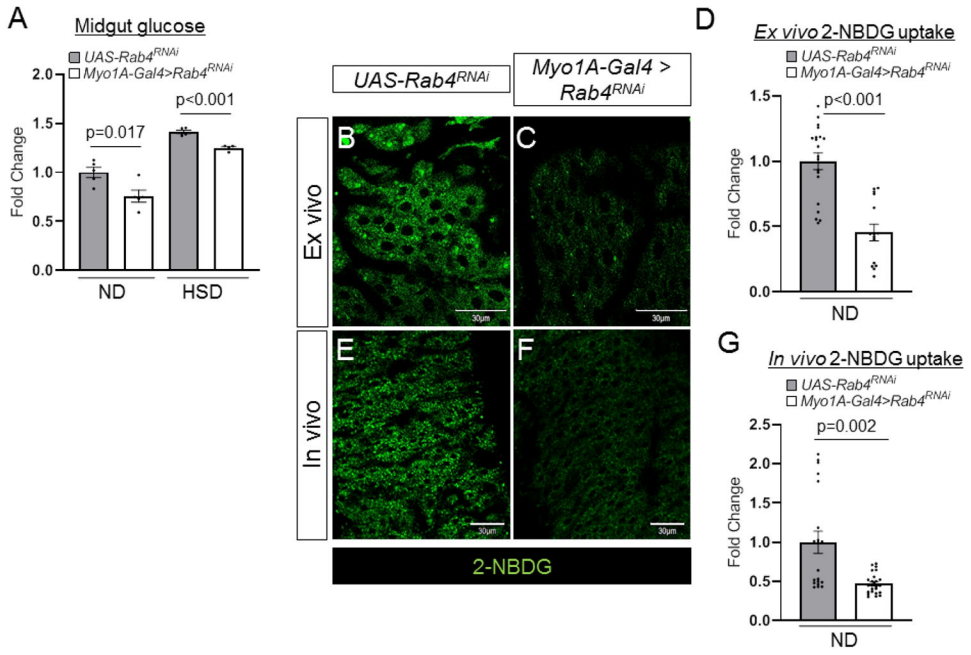

Figure 5. Midgut-specific knockdown of *Rab4* disrupts glucose uptake in the enterocytes.

(A) Midgut glucose levels in transgene control (*UAS-dTMEM214*^{RNAi}) or in *dTMEM214*-knocked down flies by *Myo1A-Gal4*. Midgut glucose levels (μg/μl) were normalized to total protein of midguts (μg/μl). (N=4-5 dots/bar, n=48-60 midguts, mean±SEM). (B-C, E-F) Representative confocal images of the intracellular accumulation of 2-NBDG in the *ex-vivo* (B-C) or *in-vivo* (E-F) enterocytes of transgene control flies (*UAS-Rab4*^{RNAi}) (B, E) or in *Rab4*-knocked down flies by the *Myo1A-Gal4* driver (C, F). Scale bars represent 30 μm. (D, G) Quantification of 2-NBDG fluorescence with the mean intensity for the different genotypes normalized to that of transgene control flies (*UAS-dTMEM214*^{RNAi}; set at 1.0) in *ex-vivo* enterocyte assay (D) or *in-vivo* enterocyte assay (G). (N=15-24 dots/bar, n=6-8 midguts with 2-3 areas per midgut quantified, mean±SEM). The R4-R5 midgut region was quantified. Two-tailed Student's *t*-test was used to derive *p*-values between the transgene control and knockdown flies. ND, normal diet, HSD, high sugar diet.

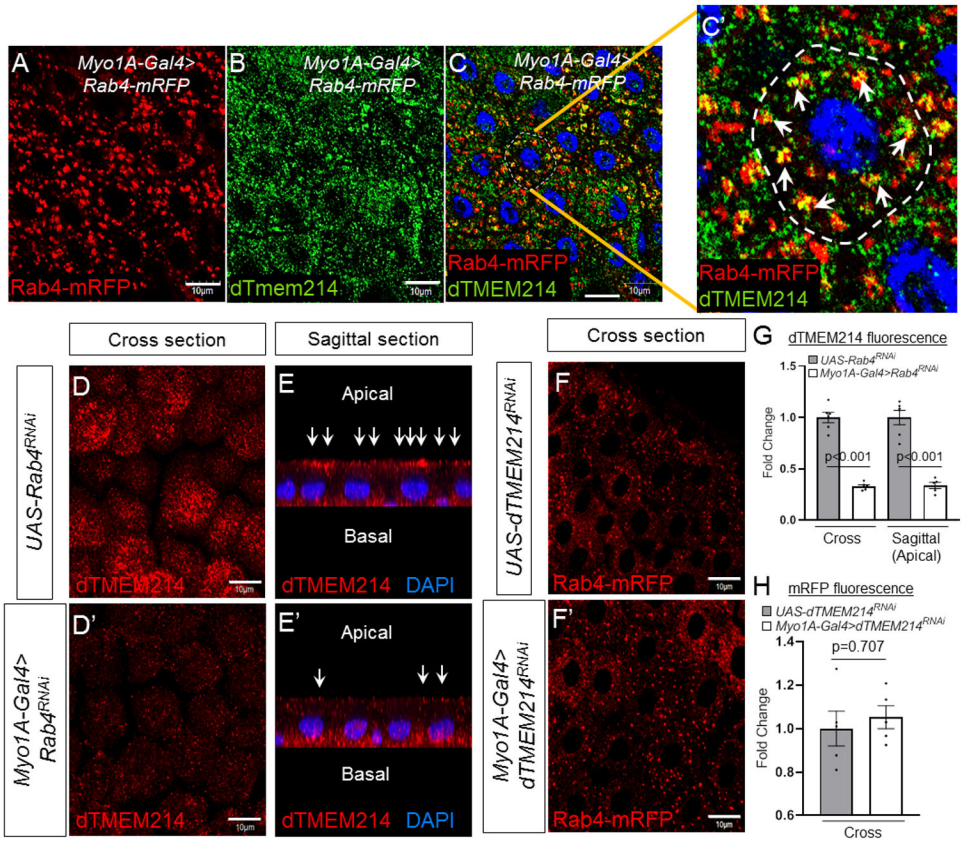

Figure 6. Rab4 co-localizes with and regulates the subcellular distribution of dTMEM214 in enterocytes

(A-C') Representative confocal images of *Myo1A-Gal4*-mediated *Rab4-mRFP* overexpressing enterocytes stained for mRFP (red, A and C), dTMEM214 (green, B and C) and DNA (blue, C). Scale bars represent 10 μm. White dashed circle indicates a single enterocyte in which colocalization of Rab4 and dTMEM214 are denoted by white arrows in inset (C'). (D-D') Representative confocal images of dTMEM214 (red) in the plasma membrane of enterocytes in transgene control flies (D) or *Myo1A-Gal4*-mediated *Rab4* knockdown flies (D') under cross-sectional view. Scale bars represent 10 μm. (E-E') Representative confocal images of dTMEM214 (red) in the plasma membrane of enterocytes in transgene control flies (D) or *Myo1A-Gal4*-mediated *Rab4* knockdown flies (D') under sagittal view. Scale bars represent 10 μm. White arrows indicate dTMEM214 in the apical membrane of enterocytes. (F-F') Representative confocal images of Rab4-mRFP (red) in enterocytes of transgene control flies (E) or *Myo1A-Gal4*-mediated *dTMEM214* knockdown flies (F). Scale bars represent 10 μm. (G) Quantification of dTMEM214 fluorescence with the mean intensity for the different genotypes normalized to that of transgene control flies (*UAS-dRab4*^{RNAi}; set at 1.0) for cross section (Figures 6D-6D') and sagittal section (apical membrane, Figures 6E-6E') of the midguts (N=5-6 dots/bar, n=2-3 midguts with 2-3 different areas per midgut quantified, mean±SEM). (H) Quantification of mRFP fluorescence with the mean intensity for the different genotypes normalized to that of transgene control flies (*UAS-dTMEM214*^{RNAi}) set at 1.0) for cross section (Figures 6f-6f') of the midguts (N=5 dots/bar, n=2-3 midguts with 1-3 areas per midgut quantified,

mean±SEM). Two-tailed Student's *t*-test was used to derive *p*-values between the transgene control and knockdown flies.

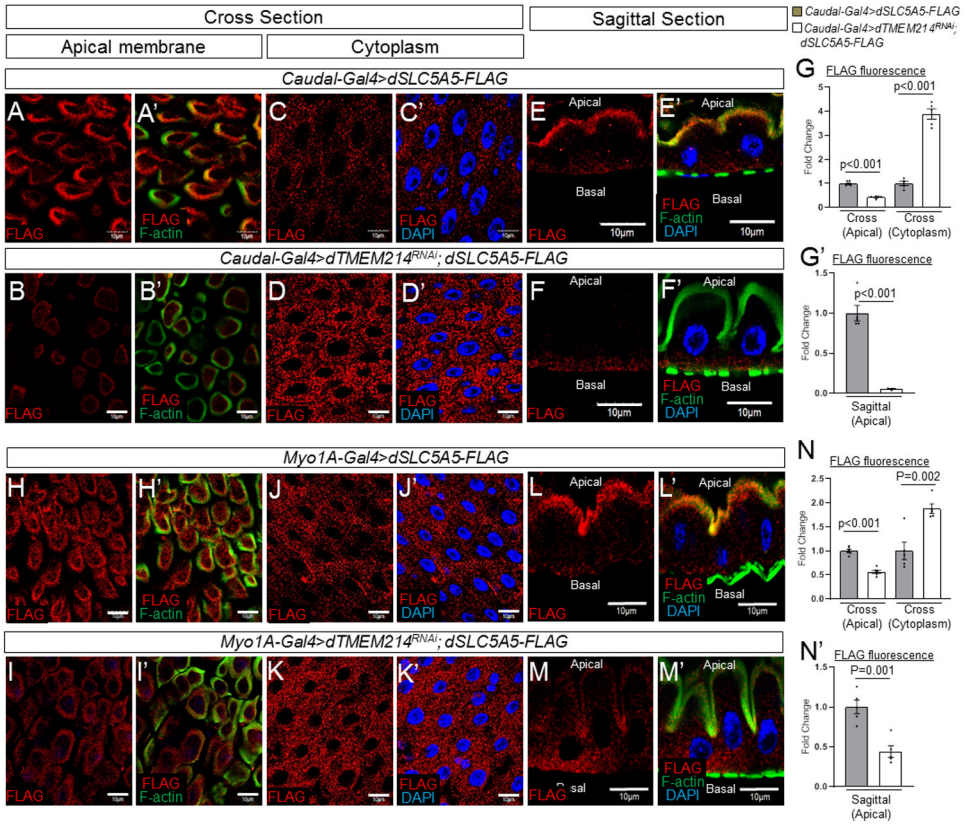

Figure 7. dTMEM214 co-localizes with dSLC5A5 and regulates the proper subcellular localization of dSLC5A5 in the midgut enterocytes

(A-D') Representative confocal images of FLAG (red), F-actin (green) and DNA (blue) immunostainings in the apical membrane (A-B') or cytoplasm (C-D') of *Caudal-Gal4*-mediated *dSLC5A5-FLAG* overexpressing enterocytes (A-A', C-C') or *Caudal-Gal4*-mediated *dSLC5A5-FLAG* overexpressing, *dTMEM214* knockdown enterocytes (B-B', D-D') under cross-sectional view. Scale bars represent 10 μm. (E-F') Representative confocal images of FLAG (red), F-actin (green) and DNA (blue) immunostainings of *Caudal-Gal4*-mediated *dSLC5A5-FLAG* overexpressing enterocytes (E-E') or *Caudal-Gal4*-mediated *dSLC5A5-FLAG* overexpressing, *dTMEM214* knockdown enterocytes (F-F') under sagittal view. Scale bars represent 10 μm. (G) Quantification of FLAG fluorescence with the mean intensity for the different genotypes normalized to that of control flies (*Caudal-Gal4>dSLC5A5-FLAG*; set at 1.0) for cross section (apical membrane, Figures 7A and 7B), cross section (cytoplasm, Figures 7C and 7D), and sagittal section (apical membrane, Figures 7E and 7F) of the midguts (N=5-6 dots/bar, n=2-3 midguts with 2-3 different areas per midgut quantified, mean±SEM). (H-M') Representative confocal images of FLAG (red), F-actin (green) and DNA (blue) immunostainings in the apical membrane (H-I) or cytoplasm (J-K') of *Myo1A-Gal4*-mediated *dSLC5A5-FLAG* overexpressing enterocytes (H-H', J-J') or *Myo1A-Gal4*-mediated *dSLC5A5-FLAG* overexpressing, *dTMEM214* knockdown enterocytes (I-I', K-K') under cross-sectional view. Scale bars represent 10 μm. (L-M') Representative confocal images of FLAG (red), F-actin (green) and DNA (blue) immunostainings of *Myo1A-Gal4*-mediated *dSLC5A5-FLAG* overexpressing enterocytes (L-L') or *Myo1A-Gal4*-mediated *dSLC5A5-FLAG* overexpressing, *dTMEM214* knockdown

enterocytes (M-M') under sagittal view. Scale bars represent 10 μm. (N-N') Quantification of FLAG fluorescence with the mean intensity for the different genotypes normalized to that of control flies (*Caudal-Gal4>dSLC5A5-FLAG*; set at 1.0) for cross section (apical membrane, Figures 7A and 7B), cross section (cytoplasm, Figures 7C and 7D), and sagittal section (apical membrane, Figures 7E and 7F) of the midguts (N=5-6 dots/bar, n=2-3 midguts with 2-3 different areas per midgut quantified, mean±SEM). Two-tailed Student's *t*-test was used to derive *p*-values between the dSLC5A5-overexpressing and dSLC5A5-overexpressing, dTMEM214-knockdown flies.